

Multi-Scale Analysis of Mechanical Properties of *Arabidopsis Thaliana* VASCULAR-RELATED NAC-DOMAIN7

Robin M. McDonald

September 25, 2020

Roumeli Research Group, University of Washington
Collaborators: Daraio Research Group and
Ravichandran Research Group, Caltech
Mentor: Dr. Eleftheria Roumeli

Abstract

Biological-matrix materials (BMMs) offer a competitive replacement for fossil fuel-based materials with greater sustainability. BMMs incorporate biological bulk matter and biopolymers, yet the biomechanical properties of the components are not well understood. Using a multi-scale approach, we aim to characterize the structural and mechanical properties of the plant bulk matter, in this case using a model cell culture system of transgenic VASCULAR-RELATED NAC-DOMAIN7 (VND7) *Arabidopsis thaliana* cells that differentiate into protoxylem vessel elements upon dexamethasone induction. We used optical microscopy to characterize the heterogeneous plant cell morphology based off of three distinct stages of differentiation: the first stage only has the primary cell wall (PCW), the second stage has developed a secondary cell wall (SCW) as well, and the third stage has a perforated PCW and tonoplast. We performed microindentation tests in different osmolarities and differentiation stages to isolate the individual turgor pressure, cell wall, and cytoplasm contributions to the overall stiffness of VND7 cells. We further probed the cell wall at nanoscales, gaining Young's moduli measurements through atomic force microscopy (AFM). From microindentation results, turgor pressure dominates in undifferentiated cells, shown by the increased stiffness of cells in hypertonic conditions. Further, in isotonic conditions, stage three cells have comparable stiffness to the other stages, demonstrating that a fully developed SCW is stiffer than turgor pressure and cytoplasm rearrangement contributions combined. Expanding the fundamental knowledge of plant cells will enable the development of better performing BMMs.

1 Introduction

Fossil fuel-based plastics and composites dominate the manufacturing sector, leading to environmental harm through material production and disposal [1]. The development of more eco-friendly materials that are cost and performance competitive will benefit efforts towards sustainability [1, 2, 3]. Biological-matrix materials (BMMs) provide an alternative way to create materials with these benefits among other properties [4]. A special class of BMMs called Engineered Living Materials (ELMs) incorporate living cells to construct the bulk matter of a material or to modulate its performance; this allows for properties such as self-healing and self-assembling [4]. The emerging classes of BMMs include bacteria, mycelia, yeast, plant, and wood-based materials.

The lower mechanical performance of existing BMM biocomposites highlights the need for further development [3, 5]. Plant cells offer a range of mechanical properties that can extend the stiffness and bending strength currently available in other BMM biocomposites. Materials with undifferentiated plant cells in a biopolymer matrix or within mycelial networks is under development [2, 5, 6]. However, the current structure, composition, and mechanical properties of plant cells, which govern the final mechanical properties of the bulk material, are not fully elucidated [5, 7].

Plant cells are highly dynamic, with a variable primary cell wall (PCW) composed of cellulose microfibrils, hemicellulose, pectin, structural proteins, and water [7]. The composition of these components varies across each cell wall and across a cell's developmental stage [7]. In vascular plants such as *Arabidopsis thaliana*, a lignin reinforced secondary cell wall (SCW) is generated from procambrial cells into protoxylem vessel elements, progressing through a series of stages that help form the xylem in living plants [8, 11]. Both the primary and secondary cell wall provide mechanical support that requires further characterization.

Arabidopsis thaliana VASCULAR-RELATED NAC-DOMAIN7 (VND7) cells have been genetically engineered to transdifferentiate into protoxylem vessel elements upon exposure to dexamethasone (DEX) [12]. The induced gene expression results in a SCW consisting of helical cellulose bundles around the direction of growth, as well as other polymers including increased xylan hemicellulose [12]. In living plants, lignification of the secondary cell wall, programmed cell death, and autolysis would occur through a series of biochemical changes, and this cell system likely follows in a similar progression [8]. In addition to the contribution of the two cell walls, we have studied the contributions of cytoplasm rearrangement and turgor pressure to the final mechanical response of the cells. Reports of actin and microtubules creating a fibrillar cytoskeleton within *Arabidopsis thaliana* and *Zinnia elegans* demonstrate a structural role in orientating the deposition of the spiral SCW bundles around the direction of cell growth [9, 10].

Using optical microscopy, we characterized the cell culture morphology. We measured the dimensions of the round and elongated shaped cells and the SCW bundle density. We obtained stiffness measurements for plant cells in sorbitol, T87 growth medium, and water with either DEX present or absent using microindentation. Escamez and Tuominen describe 6 morphological and biochemical stages of protoxylem, but we can only visually discern three developmental stages based on the structure of the cell walls: (1) only primary cell wall, (2) both cell walls, and (3) secondary cell wall present with perforated primary cell wall [8]. The heterogeneous morphology and gradient of differentiation stage poses challenges in the

classification without the aid of biochemical probing. Analysis of atomic force microscopy measurements with a Hertz model provided Young's moduli of the cell walls, additionally confirming microindentation results. We see distinctions between AFM measurements on top of SCW bundles versus between.

Further characterization of cell morphology and mechanical response across different developmental stages and mediums will be important information to further the development of plant-based biocomposites.

2 Methods

2.1 Cell Culture

VND7 *Arabidopsis thaliana* VND7 cells were previously cultured in MS-based T87 growth media, as reported in [13]. Some of the cells were exposed to dexamethasone (DEX), inducing cell differentiation into protoxylem vessel elements. Optical microscopy and AFM measurements were tested in water while the microindentation measurements were tested in three osmotic mediums (T87 growth medium, sorbitol, and water). T87 growth media served as an isosmotic condition while sorbitol was hyperosmotic, and pure deionized water was hypoosmotic. We were able to visualize three developmental stages through the cell wall morphology, though more biochemical developmental stages have been described [8].

2.2 Optical Microscopy Morphology Identification

Images of dethamexone (DEX) induced VND7 *Arabidopsis thaliana* cells in water were taken, demonstrating the progression of differentiation. The cells had been stained with a solution of alcian blue (1% vol) in acetic acid (3 vol%), highlighting the cellulose-rich cell walls. The images were taken with an AxioScope A1 and were analysed in FIJI ImageJ. We classified cells based on stage and shape (round versus elongated). Round cells were distinguished from elongated cells by having an aspect ratio between 2:3 and 1:1. We extracted cell dimensions and counted the number of SCW bundles per area, giving us a density measurement.

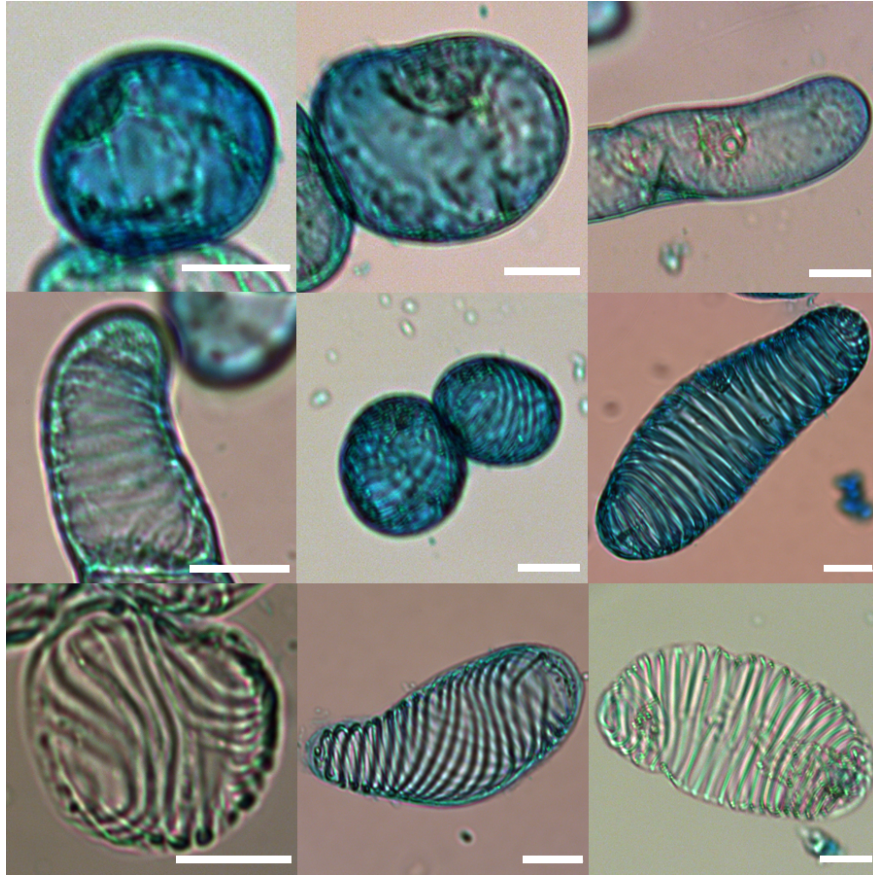


Figure 1: Examples of turgid VND7 cells in different developmental stages. Stage 1: primary cell wall is present (Top). Stage 2: primary and secondary cell walls are present (Middle). Stage 3: matured secondary cell wall with digested cytoplasm and autolyzed of primary cell wall (Bottom). Images obtained by Dr. Roumeli. All scale bars = 20 μm .

2.3 Microindentation

Roumeli had previously performed microindentation tests and collected optical images according to [13]. The FemtoTools FT-S1000-LAT microindenter has a sensing probe with a $50 \times 50 \mu\text{m}^2$ square tip. We gave the cell tests unique IDs and categorized them based on the three possible osmotic medias and DEX treatment. Roumeli previously found that the length of cell culture does not readily predict cell developmental stage, so each tested cell was visually categorized based on the microindentation optical camera images. Using FIJI ImageJ, we used the Roumeli Size Macros to measure the cell diameter (or length and width), cell area, and tip contact area. Multiple measurements per cell were taken and averaged.

The force-indentation curves were corrected by a reference measurement consisting of the respective media on a glass slide, according to [13]. Then we determined the contact point between the probe and the cell response by adjusting the force threshold, i.e. the amount of force above the baseline [14]. We truncated the baseline to reduce unnecessary noise in our measurements. The first $1 \mu\text{m}$ was linearly fit, isolating the elastic response of the cell from any possible plastic energy dissipation. This provided the stiffness response (N/m) of

the cells.

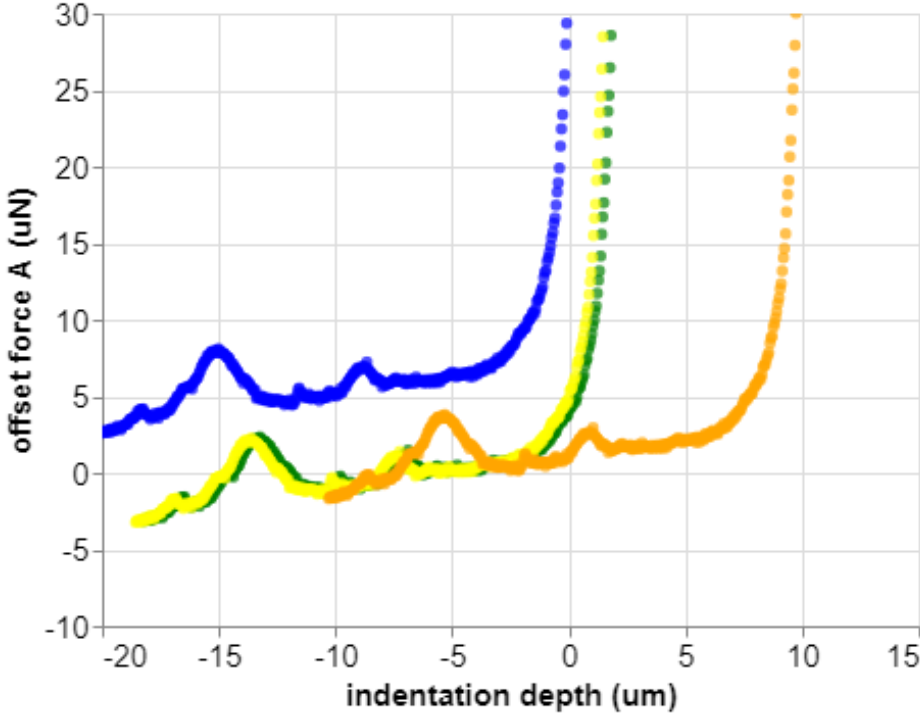


Figure 2: A range of force thresholds were used to identify when indentation begins from the baseline. Pictured are thresholds of $20 \mu\text{m}$ (blue), $10 \mu\text{m}$ (green), $5 \mu\text{m}$ (yellow), and $1 \mu\text{m}$ (orange). A threshold of $20 \mu\text{m}$ is preemptive while threshold of $1 \mu\text{m}$ over corrects the desired alignment at $0 \mu\text{m}$.

2.4 Atomic Force Microscopy

Previously, AFM tests were performed in deionized water to probe the cell walls using the Asylum Research MFP-3D-Bio with a custom, silicon dioxide spherical tip (diameter $1 \mu\text{m}$) and a silicon nitride (SN) cantilever with a stiffness of 0.6 N/m [13]. The tests had a force maximum of 3 nN , and we applied the Hertz model to calculate the Young's modulus using the Amscope AFM Software in Igor Pro:

$$F = \frac{4E}{3(1-\nu^2)} \sqrt{R\delta_0^3}$$

Adding in the force (F in nN), Poisson's ratio for the silica bead ($\nu = 0.19$), radius of the probe ($R = 0.5 \mu\text{m}$), and the indentation depth (δ_0 in nm) allowed us to obtain the Young's modulus (E in N/m^2). We used the Hertz model to fit the AFM loading curves.

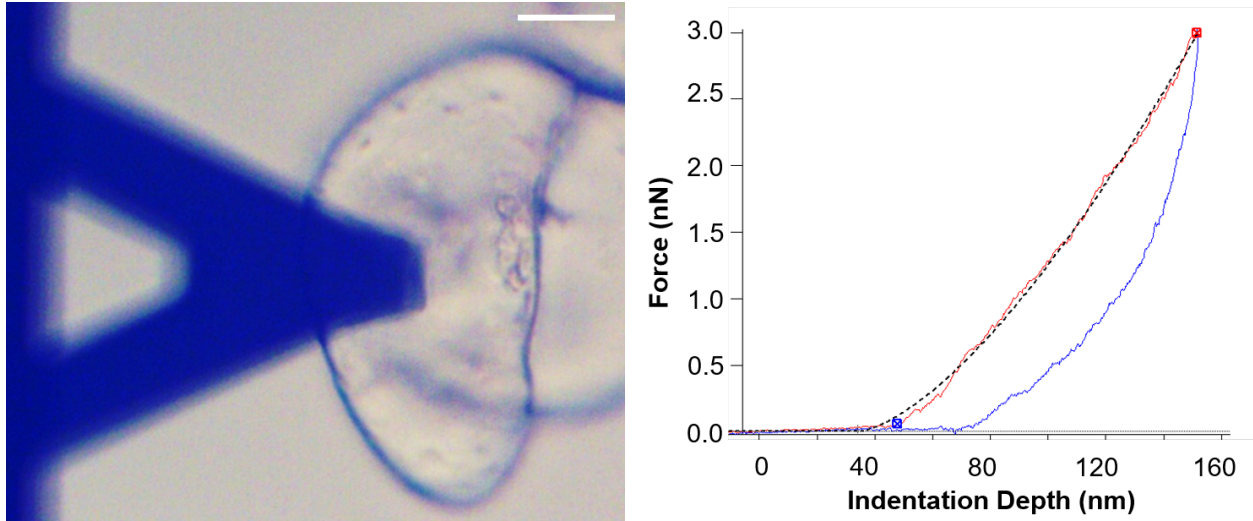


Figure 3: AFM image and plot of a cell in stage 1. The spherical silica tip under the cantilever indents until the force reaches 3 nN. The Hertz Model fits the red loading curve, and the area between curves gives the dissipated energy of deformation. Scale bar = 20 μm .

We extracted E from individual tests and maps to get a distribution of moduli across the stages of protoxylem differentiation. We also matched the AFM maps to the surface features of the cells.

3 Results and Discussion

3.1 Morphological Observations

From optical microscopy images, we primarily observed two cell types: round and elongated cells in about equal population. The round cells, especially in stage 1, tended to cluster while the elongated cells were isolated or at the edges of clusters. Some cells shared a primary cell wall, each with its separate cytoplasm, illustrating the cells were in the process of dividing. The greatest variation was in the elongated cell length, with some cells growing longer than 100 μm . On average, stage 3 round cells have a 22% larger diameter than stage 1 cells, suggesting their expansion during differentiation due to SCW deposition and PCW weakening. There is not an apparent gap between stage 2 and stage 3 round cell diameters, indicating little expansion. With elongated cells, there is not a large difference between stage 1 and stage 3 cells in dimension.

Cell Shape & Stage	Dimension	Mean \pm SE
Elongated Stage 1	Length (μm)	60.4 ± 2.4
Elongated Stage 2	Length (μm)	56.4 ± 4.9
Elongated Stage 3	Length (μm)	61.6 ± 3.7
Elongated Stage 1	Width (μm)	30.7 ± 1.0
Elongated Stage 2	Width (μm)	31.2 ± 2.8
Elongated Stage 3	Width (μm)	34.7 ± 1.6
Round Stage 1	Diameter (μm)	37.0 ± 0.9
Round Stage 2	Diameter (μm)	44.2 ± 2.1
Round Stage 3	Diameter (μm)	45.0 ± 2.0

Table 1: Dimensions of elongated and round cells. Length, width, and diameter were measured from optical microscopy images using FIJI ImageJ; n>20 per category.

We also measured the density of SCW bundles for stage 2 and stage 3 cells. This measurement gives insight into how tightly wrapped the SCW bundles are during differentiation. The differences between stage 2 and 3 densities are not significant. The bundle density is generally higher in elongated cells than rounded cells by about 7%, suggesting a higher structural requirement of elongated cell walls to support the same amount of pressure experienced by round cell walls [13].

Cell Shape & Stage	Dimension (μm)	Mean \pm SE
Elongated Stage 2	bundle density ($\#/ \mu\text{m}^2$)	0.056 ± 0.005
Elongated Stage 3	bundle density ($\#/ \mu\text{m}^2$)	0.060 ± 0.004
Round Stage 2	bundle density ($\#/ \mu\text{m}^2$)	0.051 ± 0.005
Round Stage 3	bundle density ($\#/ \mu\text{m}^2$)	0.050 ± 0.008

Table 2: SCW bundle densities for elongated and rounded cells. Bundle densities were measured from optical microscopy images and analyzed with FIJI ImageJ; n>45 per category.

3.2 Micro-Indentation Results

Testing cells in three osmotic conditions, with and without DEX treatment allowed us to isolate the contribution of turgor pressure, cytoplasm rearrangement, and cell walls to the overall cell stiffness. In addition to the three stages of differentiation, distinguished by optical microscopy observation, we designated a stage zero that refers to cells tested before any exposure to DEX. Stage 0 cells thus lacked cytoplasm rearrangement from the cytoskeleton, known to guide SCW deposition.

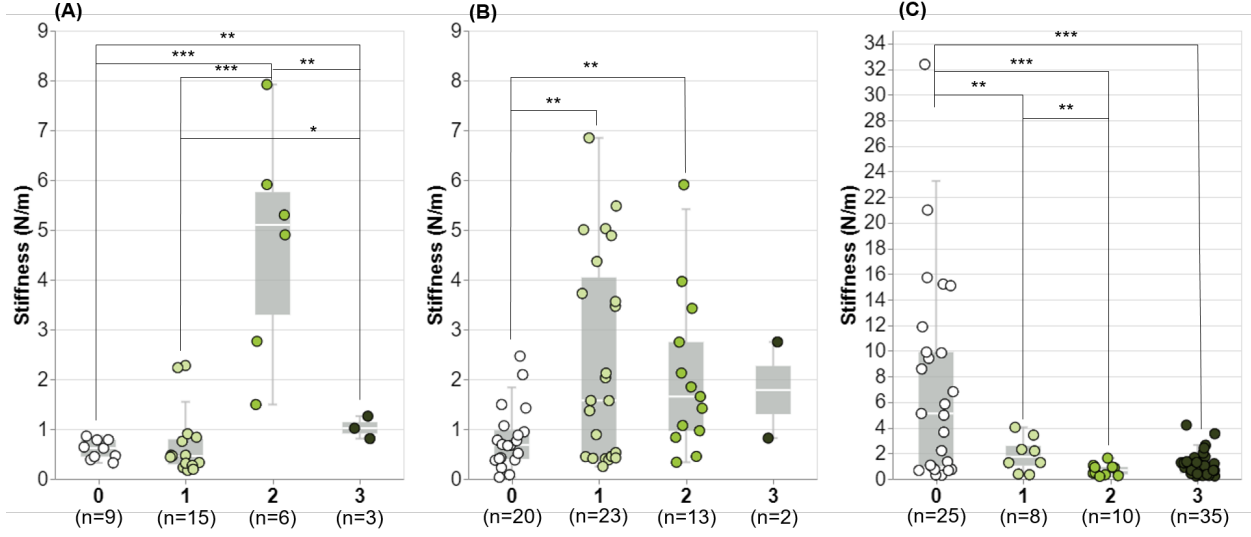


Figure 4: Stiffness measurements of differentiating cells tested in three osmotic conditions: (A) sorbitol, (B) T87 growth medium, and (C) water. The different y-axis scaling highlights the significantly higher stiffness response of cells in water before DEX treatment. Stars indicate significant differences in distribution according to a Kolmogorov-Smirnov test. * $p<0.1$, ** $p<0.05$, *** $p<0.01$. Jitter boxes are courtesy of Leah Ginsberg [13].

In the hypertonic sorbitol media, stage 2 is the stiffest. Due to cell plasmolysis, the cell wall(s) is the primary component of overall cell stiffness with diminished cytoplasm and turgor pressure effects. With the contribution of both the primary and secondary cell wall, we see that stage 2 is the stiffest. The interaction of the two cell walls leads us to propose two possible explanations. First, the sorbitol could act as a hydrogen bonding linkage between the cellulose-rich PCW and SCW. Secondly, the reduced internal support could create cell wall buckling or folding, leading to more material under the indenter and thus a greater stiffness measurement. Both explanations may be at play, leading to the increased response for stage 2 plasmolyzed cells. In addition, stage 3 is stiffer than stage 0 and stage 2, demonstrating that the mature SCW alone is stiffer than the primary cell wall alone.

The cells in the isotonic media have less variation across the stages. Between stage 0 and 1, there is some increase in stiffness, which can be attributed to cytoplasm rearrangement. Comparing stages 1, 2, and 3, we see no significant differences in stiffness. In stage 1 we have cytoplasm, turgor pressure (at equilibrium with the media), and PCW support. As the cell develops a SCW in stage 2, a combination of PCW loosening for growth and some internal cytoplasm digestion is in opposition with the strength provided by the developing SCW. Then in stage 3, only the SCW contributes, meaning the fully developed SCW is as stiff as the combined cytoplasm, neutral turgor pressure, and PCW. As biomass is primarily secondary cell wall, the quantification of the stiffness response of the SCW alone is important to us and demonstrates its structural role [15].

In the hypotonic media, stage 0 has cases with stiffness far exceeding the other conditions. The swollen vacuole's turgor pressure stresses the PCW the most, dominating the mechanical response. Subsequently, the stiffness decreases due to PCW weakening, loss of turgor, and digestion of cytoplasm. Stage 3 has higher stiffness than stage 2, supporting the result that

mature SCW is stiffer than the individual contributors during stage 2.

Our biomechanical assay enables the isolation of cell wall and turgor pressure contributions, as well as assessing the mechanical response of the cytoskeleton for the first time in intact plant cells. The role of the cytoplasm rearrangement, turgor pressure, and cell walls all play various roles during differentiation.

3.3 Atomic Force Microscopy

Through nanoindentation, we probed to a force of 3 nN which gave us an indentation depth of several tens of nm using a spherical tip of diameter 1 μm . We chose this tip because the SCW bundles are known to have a thickness of 5-50 nm [16]. The tests were conducted in water, and we extracted the Young's moduli from individual tests as well as stiffness maps that match the cell features.

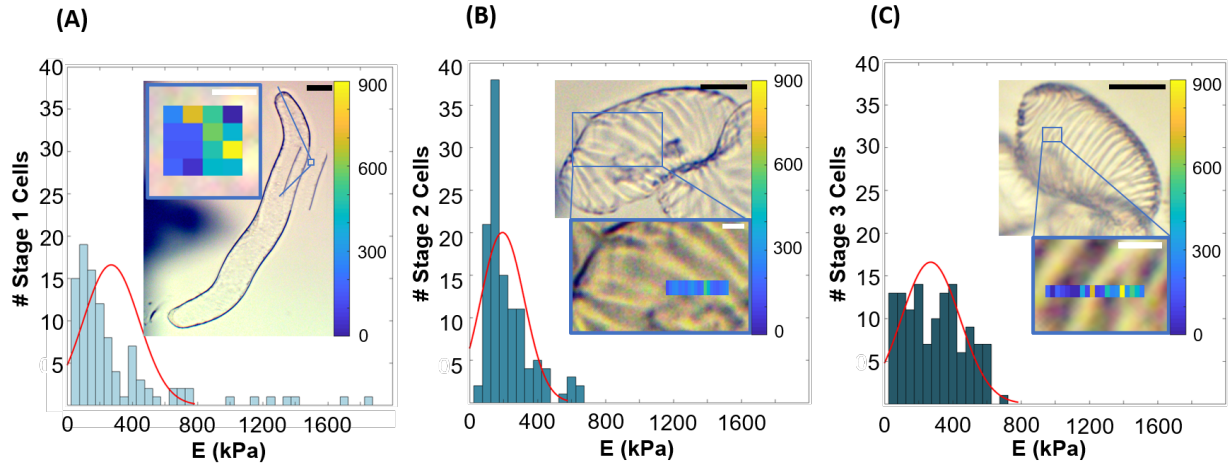


Figure 5: AFM isolates the response of the cell wall and can map the anisotropic features. (A) Distribution of stage 1 cells' E with an example map showing the PCW, (B) distribution of stage 2 cells' E with example line scan showing both cell wall features, and (C) distribution of stage 3 cells' E with a line scan showing the mature SCW features. White scale bars = 5 μm ; black scale bars = 20 μm .

These results match our hypotonic microindentation results where the response is stiffest in stage 1 ($E=372\pm51$ kPa) and least stiff in stage 2 ($E = 192\pm13$ kPa). The average Young's modulus in stage 3 ($E=271\pm15$ kPa) is between, further validating our microindentation results. There is the greatest spread in stage 1, reflecting the anisotropic behavior of the PCW, stressed by turgor pressure. In stage 2, the weaker response of the combined cell walls can be explained by measurements taken over weakened PCW. It is observed that the Young's moduli are higher on top of the stiffer SCW bundles versus the weakened PCW. From the example insert, the SCW has about a response of 550 kPa while the weakened PCW in between averages 220 kPa. The distribution of stage 3 cells are more uniform. As the SCW matures, it thickens, filling in the inner-bundle spaces and reducing weakened PCW measurements [13]. Overall, the AFM confirms the highly heterogeneous morphology and

anisotropic nature of these cells, with the SCW stronger than weakened PCW in hypotonic media.

4 Conclusion

This multi-scale analysis of transgenic VND7 *Arabidopsis thaliana* cells has furthered our fundamental knowledge of the mechanical properties and structure of plant cells as well as informed future biocomposite creation. Since SCW dominates vascular plant composition, we wanted to understand its mechanical contributions as well as directly isolate the components of turgor pressure and cytoplasm rearrangement. We found that the the structure of these plant cells are highly heterogeneous, ranging from the shape of the cell to the changing Young's modulus across a cell wall. Despite challenges in characterization, these cells' ability to organize a host of polymers into a helical-patterned SCW offers the potential benefit of stiffening biological-matrix materials in the future.

References

- [1] Mohanty, A.; Vivekanandhan, S.; Pin, J.M.; Misra,M. (2018). Composites from renewable and sustainable resources: Challenges and innovations, *Science*, 362(6414), 536-542, doi:10.1126/science.aat9072
- [2] Bourmaud, A.; Beaugrand, J.; Shah, D.U.; Placet, V.; Baley, C. (2018). Towards the design of high-performance plant fibre composites. *Prog. Mater. Sci.* 97, 347–408. doi: 10.1016/j.pmatsci.2018.05.005
- [3] Pickering, K.L; Efendi, M.A.; Le, T.M. (2016). A review of recent developments in natural fibre composites and their mechanical performance. *Compos. A* 83, 98–112. doi: 10.1016/j.compositesa.2015.08.038
- [4] Nguyen, P.Q.; Courchesne, N.D.; Duraj-Thatte, A.; Praveschotinunt, P.; Joshi, N.S. (2018). Engineered Living Materials: Prospects and Challenges for Using Biological Systems to Direct the Assembly of Smart Materials. *Advanced materials*, 30(19), e1704847. <https://doi.org/10.1002/adma.201704847>
- [5] Roumeli, E.; Bonanomi, L.; Hendrickx, R.; Rinaldi, K.; Daraio, C. (2019). Plant cells-based biological matrix composites. *arXiv* :1909.01926
- [6] Haneef, M.; Ceseracciu, L.; Canale, C. et al. Advanced Materials From Fungal Mycelium: Fabrication and Tuning of Physical Properties. *Sci Rep* 7, 41292 (2017). <https://doi.org/10.1038/srep41292>
- [7] Bidhendi, A.; Geitmann, A. (2019). Methods to quantify primary plant cell wall mechanics. *Journal of Experimental Biology*, 70(14), 3615-3648
- [8] Escamez, S.; Tuominen, H. (2014). Programmes of cell death and autolysis in tracheary elements: when a suicidal cell arranges its own corpse removal, *Journal of Experimental Botany*, 65(5), 1313–1321, <https://doi.org/10.1093/jxb/eru057>
- [9] , Y.; Meents, M.J.; McDonnell, L.M.; Barkwill, S.; Sampathkumar, A.; Cartwright, H.N.; Demura, T.; Ehrhardt, D.W.; Samuel, A.L.; Mansfield, S.D. (2015). Visualization of cellulose synthases in *Arabidopsis* secondary cell walls, *Science*, 350(6257), 198-203, doi: 10.1126/science.aac7446
- [10] Fukuda, H.; Kobayashi, H. (1989). Dynamic Organization of the Cytoskeleton during Tracheary-Element Differentiation, *Develop Growth Differ*.31(1), 12-1592, <https://doi.org/10.1111/j.1440-169X.1989.00009.x>
- [11] Smith, R.A. (2014). Good neighbours: the role of non-lignified cells in *Arabidopsis* lignification (T). University of British Columbia. Retrieved from <https://open.library.ubc.ca/collections/ubctheses/24/items/1.0167289>
- [12] Yamaguchi, M.; Goué, N.; Igarashi, H.; Ohtani, M.; Nakano, Y.; Mortimer, J.C.; Nishikubo, N.; Kubo, M.; Katayama, Y.; Kakegawa, K.; Dupree, P.;

- Demura, T. (2010). VASCULAR-RELATED NAC-DOMAIN6 and VASCULAR-RELATED NAC-DOMAIN7 effectively induce transdifferentiation into xylem vessel elements under control of an induction system. *Plant physiology*, 153(3), 906–914. <https://doi.org/10.1104/pp.110.154013>
- [13] Roumeli, E.; Ginsberg, G.; McDonald, R.; Spigonlon, G.; Rodine, H.; Ohtani, M.; Demura, T.; Ravichandran, G.; Daraio, C.; (2020), Structure and biomechanics during xylem vessel transdifferentiation in *Arabidopsis thaliana*, *in progress*
- [14] Bonilla, M.R.; Stokes, J.R.; Gidley, M.J.; Yakubov, G.E. (2015). Interpreting atomic force microscopy nanoindentation of hierarchical biological materials using multi-regime analysis, *Soft Matter*, 2015,11, 1281-1292, <https://doi.org/10.1039/C4SM02440K>.
- [15] Kang, X.; Kirui, A.; Dickwella Widanage, M.C.; Mentink-Vigier, F.; Cosgrove, D.J.; Wang, T. (2019). Lignin-polysaccharide interactions in plant secondary cell walls revealed by solid-state NMR, *Nat Commun* 10(347) (2019), <https://doi.org/10.1038/s41467-018-08252-0>
- [16] Moon, R.J.; Martini, A.; Nairn, J.; Simonsen, J.; Youngblood, J. (2011). Cellulose nanomaterials review: structure, properties and nanocomposites. *Chem. Soc. Rev.*, 40, 3941–3994, doi:10.1039/C0CS00108B.4384